

Paper:

# Observation of Thermal Influence on Error Motions of Rotary Axes on a Five-Axis Machine Tool by Static R-Test

Cefu Hong and Soichi Ibaraki

Department of Micro Engineering, Graduate School of Engineering, Kyoto University  
Yoshida-honmachi, Sakyo-ku, Kyoto 606-8501, Japan  
E-mail: c.hong@fs8.ecs.kyoto-u.ac.jp

[Received August 25, 2011; accepted November 22, 2011]

Thermal distortions are regarded as one of the major error factors in machine tools. ISO 230-3 and ISO 10791-10 describe tests to evaluate the influence of thermal distortions caused by linear motion and spindle rotation on the Tool Center Position (TCP). However, for five-axis machine tools, no thermal test is described for a rotary axis. Therefore, in this paper, a method for observing thermally induced geometric errors of a rotary axis with a static R-test is proposed. Unlike conventional thermal tests in ISO 230-3 and ISO 10791-10, where the thermal influence on the positioning error at a single point is tested, the present test measures the thermal influence on the error motions of a rotary axis. The R-test measurement clarifies how the error motions of a rotary table change with the rotation of a swiveling axis and how they are influenced by thermal changes. The thermal influence on the error motions of a rotary axis is quantitatively parameterized by geometric errors that vary with time.

**Keywords:** error motion of rotary axes, thermal test, R-test, five-axis machine tool, geometric error

## 1. Introduction

A five-axis machine tool is composed of three orthogonal linear axes and two rotary axes. With the ability to control the orientation of a tool with respect to a workpiece, five-axis machine tools can machine geometrically complex workpieces with potentially higher efficiency. However, to meet the increasing need for higher accuracy five-axis machining, improvement of the motion accuracy of five-axis machine tools is becoming a crucial issue in the market.

Many researchers have recently reported calibration schemes for kinematic errors in a five-axis machine tool by using, e.g., the ball bar [1–3]. However, a method of evaluating the thermal influence on five-axis kinematics is rarely found in the literature. Among many error sources in machine tool kinematics, thermal errors can be one of the dominant error factors under extended usage of the machine [4, 5].

ISO 230-3 and ISO 10791-10 [6, 7] describe tests to

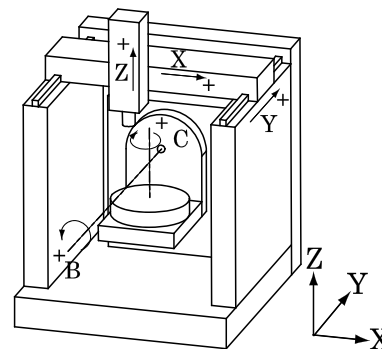


**Fig. 1.** Configuration of a five-axis machine tool considered in this paper.

evaluate thermal distortions on machine tools caused by a rotating spindle and the reciprocating motion of linear axes. No test is described in these standards on the thermal influence on a rotary axis. Furthermore, conventional thermal tests only measure the thermal influence on the TCP (Tool Center Position) and its orientation; they do not evaluate the error motions of an axis. In serial-link kinematics, the error motions of one axis are often affected by those of the axis on which it is mounted. For example, in the tilting rotary table configuration (see **Fig. 1**), where a rotary table (*C*-axis) is installed on a swiveling axis (*B*-axis), error motions of the *C*-axis are often influenced by the angular position of the *B*-axis due to, e.g., gravity-induced deformation. Thermal deformation may change the dependency of the *C*-axis error motions on the *B*-axis angular position.

The objective of this research is to propose a method to observe the influence of thermal distortions on the error motions of a rotary axis in five-axis kinematics.

As was discussed in [8], the effect of thermal errors can be incorporated into the kinematic error model of five-axis machine tools as thermally-induced geometric errors. For the calibration of geometric errors associated with rotary axes, Weikert [9] and Bringmann and Knapp [10] presented the “R-Test,” where the three-dimensional displacement of a sphere attached to the spindle is measured by three (or four in [9, 10]) linear displacement sensors installed on the table. Similar to ball bar tests, ISO TC39/SC2 discussed the inclusion of the R-test in the re-

vision of ISO 10791-6 [11]. Commercial R-test devices are now available from IBS Precision Engineering [12] and Fidia [13]. A similar measurement device composed of capacitance sensors, called “Capball,” was proposed in [14].

Past works [10, 14] focused on the application of the R-test to calibrate the location errors of rotary axes. In ISO 230-7 [15], the location errors of a rotary axis are defined as position and orientation errors of its axis average line, i.e., the straight line segment located with respect to the reference coordinate axes that represents the mean location of the axis of rotation. In other words, location errors only represent the average error in the position and orientation of the axis of rotation. In many recent five-axis machine tools, it is of a practical importance to calibrate not only the average of the error motions of a rotary axis but also how the error motion changes with its rotation. Such error motions are parameterized as a function of the angular position of a rotary axis and are represented by component errors in ISO230-7 [15] or as an “error map” of the five-axis kinematics [16]. The dependency of the C-axis error motions on the B-axis angular position can be parameterized as such component errors. In this paper, the location errors and component errors of a rotary axis are together called geometric errors [5].

To intuitively observe geometric errors of rotary axes, the authors proposed a graphical presentation of displacement profiles measured by an R-test in [17]. An algorithm to identify not only location errors but also position-dependent component errors of rotary axes with a static R-test was proposed in [16] by a part of the authors. By using the approaches proposed in [17] and [16], this paper will present a methodology to evaluate how thermal changes influence the error motions, or error map, of the rotary axes.

## 2. Measuring Instrument and Test Procedure

### 2.1. Machine Configuration

This paper considers the five-axis machine configuration with a tilting rotary table (B- and C-axes) depicted in Fig. 1. It must be emphasized that the basic idea of this paper can be straightforwardly extended to any configuration of five-axis machine.

### 2.2. R-Test Measurement Instrument

Figure 2 shows the R-test device used in this study. A ceramic precision sphere with a 25.4 mm diameter is attached to a machine spindle. Three contact-type linear displacement sensors with flat-ended probes are attached on a fixture (named the sensors nest in [16]) that is fixed on a rotary table. Table 1 shows the major specifications of the sensors.

The direction of each sensor must be pre-calibrated [9, 10, 16]. The R-test measures the sphere displacement in the workpiece coordinate system. In this paper, the coordinate system attached to the rotary table

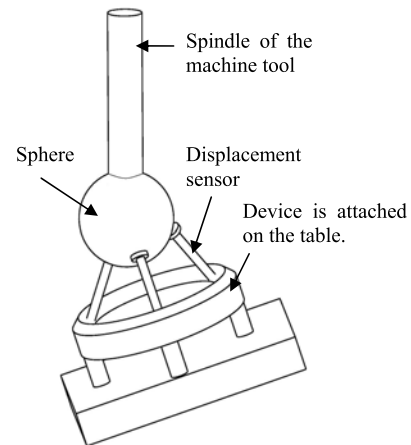


Fig. 2. Configuration of R-test device [16].

Table 1. Specifications of the linear displacement sensor.

Measuring principle	Photo-electric scanning of an incremental scale with spring-tensioned plunger
Measurement range	12 mm
System accuracy	$\pm 0.2 \mu\text{m}$
Gauging force (vertically upward)	0.35 to 0.6 N
Signal period	$2 \mu\text{m}$
Mechanically permissible traversing speed	30 m/min

is referred to as the workpiece coordinate system; the origin of the workpiece coordinate system is set to be the intersection of the nominal B-axis and C-axis. The coordinate system fixed to the machine frame or bed is called the reference coordinate system.

### 2.3. Test Procedure

#### (1) Reciprocating motion of a rotary axis

In this paper, the thermal influence of a rotary axis caused by an internal heat source will be investigated. Since the deformation of the swiveling B-axis may significantly influence error motions of the rotary table, the B-axis is naturally selected to be the reciprocating axis. The B-axis performs a reciprocating movement. Note that other axes (i.e., linear axes and C-axis) are stopped within the B-axis reciprocating motion. At the given time interval, the reciprocating motion of the B-axis is interrupted and the following R-test measurement cycle is conducted.

#### (2) R-test measurement procedure

In the R-test measurement cycle, the machine table is indexed at each combination of given B- and C-angular positions  $B_i^*$  ( $i = 1, \dots, N_b$ ) and  $C_j^*$  ( $j = 1, \dots, N_c$ ). Measurement poses  $B_i^*$  and  $C_j^*$  must be distributed over the entire workspace of each rotary axis. The X, Y, and Z axes are positioned such that there is nominally no relative displacement of the sphere to the sensors nest [16].

At each stop position  $B_i^*$  ( $i = 1, \dots, N_b$ ) and  $C_j^*$  ( $j = 1, \dots, N_c$ ) in the R-test measurement cycle, the R-test sen-

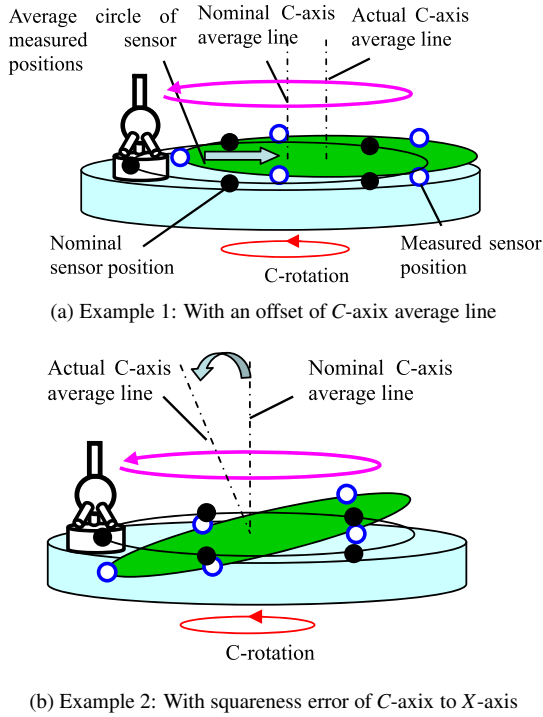


**Fig. 3.** Illustrative examples of graphical presentation of R-test measurement result.

sors nest statically measures the sphere displacement in the workpiece coordinate system, denoted by  ${}^wq(B_i^*, C_j^*)$ .

### 3. Analysis of R-Test Profiles

#### 3.1. Graphical Presentation of R-Test Profile

For a more intuitive understanding of rotary axes error motions, the authors [17] proposed displaying the measured R-test profile by transforming it to the reference coordinate system. Since the measured R-test displacement,  ${}^wq(B_i^*, C_j^*) (i = 1, \dots, N_b, j = 1, \dots, N_c)$ , represents the sphere displacement relative to the sensors nest,  $-{}^wq(B_i^*, C_j^*)$  represents the displacement of the sensors nest relative to the spindle sphere. By transforming  $-{}^wq(B_i^*, C_j^*)$  to the reference coordinate system with nominal  $B_i^*$  and  $C_j^*$ , its profile represents the error motions of the rotary table (C-axis) in reference to the spindle sphere position (i.e., the trajectory of the linear axes). This profile is called the sensor position profile measured by the R-test. Two typical examples of the sensor position profile are illustrated in **Figs. 3(a)** and **(b)**. The detailed procedure for graphical presentation of the R-test profile can be found in [17] and is not repeated here.

#### 3.2. Error Parameters of the Rotary Table to be Identified

The location and orientation of an axis of rotation may vary due to its rotation (i.e., component errors in ISO 230-7 [15]). A large class of error motions can be modeled as

**Table 2.** Description of geometric errors of a rotary table.

Symbol	Description
$\delta_{x_{BY}}(B, t)$	Location changes of B-axis of rotation in X-direction depending on B-angle and time $t$ .
$\delta_{y_{CB}}(B, t)$	Location changes of the rotary table's axis of rotation in Y-direction depending on B-angle and time $t$ .
$\delta_{z_{BY}}(B, t)$	Location changes of B-axis of rotation in Z-direction depending on B-angle and time $t$ .
$\alpha_{BY}(B, t)$	Orientation changes of B-axis of rotation around X-axis depending on B-angle and time $t$ .
$\beta_{BY}(B, t)$	Angular positioning error of B-axis of rotation depending on B-angle and time $t$ .
$\gamma_{BY}(B, t)$	Orientation changes of B-axis of rotation around Z-axis depending on B-angle and time $t$ .

geometric errors that vary depending on the angular position [16]. Moreover, as was discussed in [8], thermal distortions can be modeled by geometric errors that vary with time. The objective of the error calibration presented in this paper is to parameterize the time- and position-dependent geometric errors of a rotary table shown in **Table 2**, representing the thermal influence on error motions of the rotary table.

#### 3.3. Calibration Procedure of Geometric Errors of the Rotary Table

From each R-test profile measured at the given time interval, location errors and position-dependent geometric errors are numerically identified. The detailed algorithm is presented in [16]. Here a brief summary is presented.

##### (1) Kinematic modeling of the rotary table

When geometric errors of the rotary table are given as shown in **Table 2**, the sphere position in the workpiece coordinate system,  ${}^wq(B_i^*, C_j^*)$ , is formulated as follows:

$$\begin{bmatrix} {}^wq(B_i^*, C_j^*) \\ 1 \end{bmatrix} = {}^wT_r \begin{bmatrix} {}^r q(B_i^*, C_j^*) \\ 1 \end{bmatrix} = ({}^rT_w)^{-1} \begin{bmatrix} {}^r q(B_i^*, C_j^*) \\ 1 \end{bmatrix} \quad (1)$$

$$\begin{aligned} {}^rT_w &= {}^rT_b^b T_c \\ {}^rT_b &= D_a(\alpha_{BY}(B_i^*)) D_b(\beta_{BY}(B_i^*)) \cdot \\ &D_c(\gamma_{BY}(B_i^*)) D_x(\delta_{x_{BY}}(B_i^*)) \cdot \\ &D_y(\delta_{y_{CB}}(B_i^*)) D_z(\delta_{z_{BY}}(B_i^*)) \cdot \\ &D_b(-B_i^*) \\ {}^bT_c &= D_a(\alpha_{CB}^0) D_x(\delta_{x_{CB}}^0) D_c(-C_j^*) \end{aligned} \quad (2)$$

where  $D_x(x)$ ,  $D_y(y)$ ,  $D_z(z) \in \mathfrak{R}^{4 \times 4}$  represent the HTMs (Homogeneous Transformation Matrices) for linear motions in the X-, Y-, and Z-directions respectively, and  $D_a(a)$ ,  $D_b(b)$ ,  $D_c(c) \in \mathfrak{R}^{4 \times 4}$  represent the HTMs for angular motions about the X-, Y-, and Z-directions respectively. Their formulations are given in, e.g., [16]. For example,  ${}^rT_b \in \mathfrak{R}^{4 \times 4}$  denotes an HTM representing the

transformation from the coordinate system attached to the  $B$ -axis of rotation at the command  $B$ -angle  $B_i^*$  to the reference coordinate system. Note that the left-side  $r$  represents a vector in the reference coordinate system;  $w$  represents a vector in the workpiece coordinate system.  ${}^r q(B_i^*, C_j^*)$  represents the command sphere position in the reference coordinate system and is given as follows:

$$\begin{bmatrix} {}^r q(B_i^*, C_j^*) \\ 1 \end{bmatrix} = D_b(-B_i^*) D_c(-C_j^*) \begin{bmatrix} {}^w q^* \\ 1 \end{bmatrix} \quad (3)$$

where  ${}^w q^*$  represents the nominal sphere position in the workpiece coordinate system.

#### (2) Identification of geometric errors of the rotary table

It is important to note that R-test probes can only measure the displacement of the sphere center from its initial position (i.e., the position when  $B_i^* = C_j^* = 0^\circ$ ). After the initial resetting [16], the sphere displacement measured by the R-test probes is represented by

$${}^w \bar{q}(B_i^*, C_j^*) = {}^w q(B_i^*, C_j^*) - {}^w q(0^\circ, 0^\circ) \quad \dots \quad (4)$$

The set of geometric errors of the rotary table to be identified, shown in **Table 2**, is denoted by

$$\omega_0 = [\delta x_{BY}(B_i^*), \delta y_{CB}(B_i^*), \delta z_{BY}(B_i^*), \alpha_{BY}(B_i^*), \beta_{BY}(B_i^*), \gamma_{BY}(B_i^*)]^T \quad (5)$$

When the sphere displacement,  ${}^w \bar{q}(B_i^*, C_j^*)$ , is measured by the R-test probes,  $\omega_0$  is identified by solving the following problem with the method proposed in [16]:

$$\min_{\omega_0} \sum_{i,j} \left\| \begin{bmatrix} {}^w \bar{q}(B_i^*, C_j^*) \\ - \left( \frac{\partial ({}^w q(B_i^*, C_j^*))}{\partial \omega_0} - \frac{\partial ({}^w q(0^\circ, 0^\circ))}{\partial \omega_0} \right) \omega_0 \end{bmatrix} \right\|^2 \quad (6)$$

where  $\|\cdot\|$  represents the 2-norm. The Jacobian matrices in the formulation above can be analytically derived from Eq. (1).

### 4. Case Study

#### 4.1. Experimental Setup

In this experiment, the R-test sensors nest is installed at  $[-0.448 \text{ mm}, -91.187 \text{ mm}, 40.567 \text{ mm}]^T$  in the workpiece coordinate system (defined in section 2.2), as shown in **Fig. 4**. Five thermocouple sensors (sheathed type) are attached at the locations shown in **Fig. 4** to roughly correlate the calibrated geometric errors and thermal distribution.

The  $B$ -axis continuously swivels between  $-90^\circ$  and  $-60^\circ$  at a feedrate of 5000 degree/min. Every 15 minutes, this  $B$ -axis reciprocating motion is interrupted, and the R-test measurement cycle is conducted with the following command  $B$  and  $C$  angular positions:

$$B_i^* = -60^\circ, -30^\circ, \dots, 60^\circ (i = 1, \dots, 5)$$

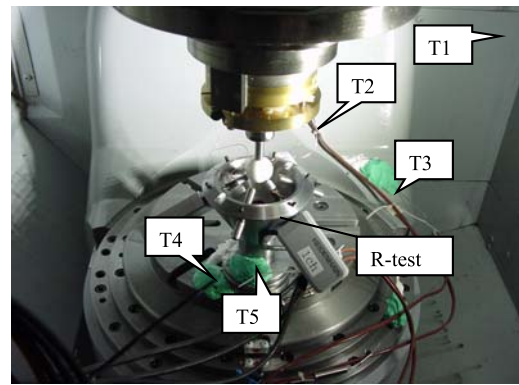


**Fig. 4.** Setup of R-test and thermocouple sensors (T1: thermocouple sensor for ambient temperature; T2: on the  $B$ -axis cover near  $B$ -axis center; T3: on the cover near bridge between  $B$ -shaft and  $C$ -table; T4: on  $C$ -table; T5: on R-test).

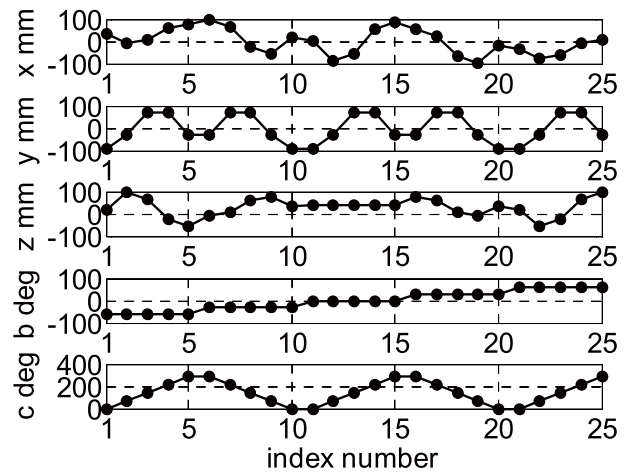


**Fig. 5.** Command  $X$ ,  $Y$ ,  $Z$ ,  $B$ , and  $C$  positions for each R-test measurement cycle.

$$C_j^* = 0^\circ, 72^\circ, \dots, 288^\circ (j = 1, \dots, 5)$$

A total of  $5 \times 5 = 25$  points are measured. **Fig. 5** shows command  $X^*$ ,  $Y^*$ ,  $Z^*$ ,  $B^*$ , and  $C^*$  trajectories for an R-test measurement cycle. One R-test measurement cycle for 25 points takes less than 2 minutes including the setup time.

#### 4.2. Measured Temperatures

**Figure 6** shows measured temperatures throughout this experiment, which continued for about 3 hours. The following observations can be made:

- The temperature on the  $B$ -axis cover near the  $B$ -axis center (T2) rose by  $1.4^\circ\text{C}$ .
- The temperature rise on the cover near the bridge between the  $B$ -shaft and  $C$ -table (T3) was about  $0.7^\circ\text{C}$ . No temperature rise on the  $C$ -table (T4) was observed. This suggests that the transfer of the heat caused by reciprocating motion of the  $B$ -axis to the surface of the rotary table was sufficiently small.

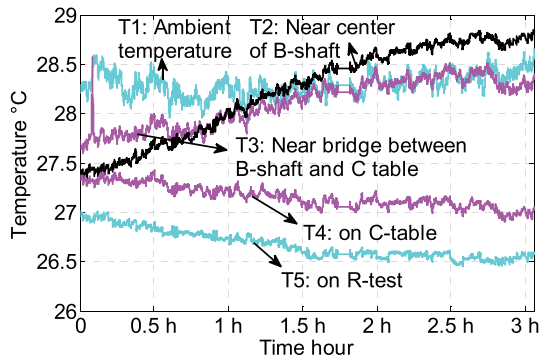


Fig. 6. Measured temperature of thermocouple sensors.

- Throughout this experiment, the change in the ambient temperature (T1) and the temperature of the R-test device (T5) were within 0.5°C.

To see the causal connection between reciprocated motions and temperature rises, as well as the error motions of rotary axes, we have conducted another experiment with different conditions of reciprocating *B*-axis motion. In this test, the *B*-axis was swiveled between  $-15^\circ$  and  $15^\circ$  at 5000 deg/min. Compared to the present test ( $-90^\circ$  to  $-60^\circ$  at 5000 deg/min), the temperature rise of the *B*-shaft was significantly smaller. In the present test, the *B*-axis motor outputs significantly larger torque due to the gravity influence. By comparing these two tests, we reasonably conclude that the temperature rise observed in Fig. 6, as well as the change in the error motions presented in the following subsection, is caused mainly by the *B*-axis reciprocating motion.

### 4.3. Graphical Presentation of R-Test Profile

#### (1) Test results

The R-test profile measured at each test interval,  ${}^wq(B_i^*, C_j^*) (i = 1 - 5, j = 1 - 5)$ , is transformed to the reference coordinate system, denoted by  ${}^r q'(B_i^*, C_j^*)$  as presented in section 3.1. Sensor position profiles measured at 0, 1, and 2 hours from the beginning of the test (denoted by time  $t = 0$  h, 1 h, 2 h) are shown as three-dimensional views in Figs. 7(a)–(c). Although the R-test cycle was conducted a total of 11 times in 3 hours, only three profiles ( $t = 0$  h, 1 h, 2 h) are shown, to simplify the plot. Note that an error in a measured position ( $\circ$ ) from its command position ( $\bullet$ ) is magnified 8000 times.

Figures 7(a), (b), and (c) present sensor position profiles measured with *C*-rotation ( $C_j^* = 0^\circ$  to  $288^\circ$ ) at  $B_i^* = -60^\circ, 0^\circ,$  and  $60^\circ$ , respectively. In each plot, three painted circles represent the average circle fit to the measured sensor positions for  $t = 0$  h, 1 h, and 2 h. These average circles are shown to facilitate easier understanding of the position and orientation of the *C*-axis average line (see Fig. 3). “Table” shows the rough position of the rotary table. Figs. 8(a)–(c) show their projections onto the *XY* plane. Figs. 9(a)–(c) show their projections onto the *XZ* plane.

It is to be noted that the static axis shift of the *B*-axis in the *Z*-direction at the start of this series of measure-

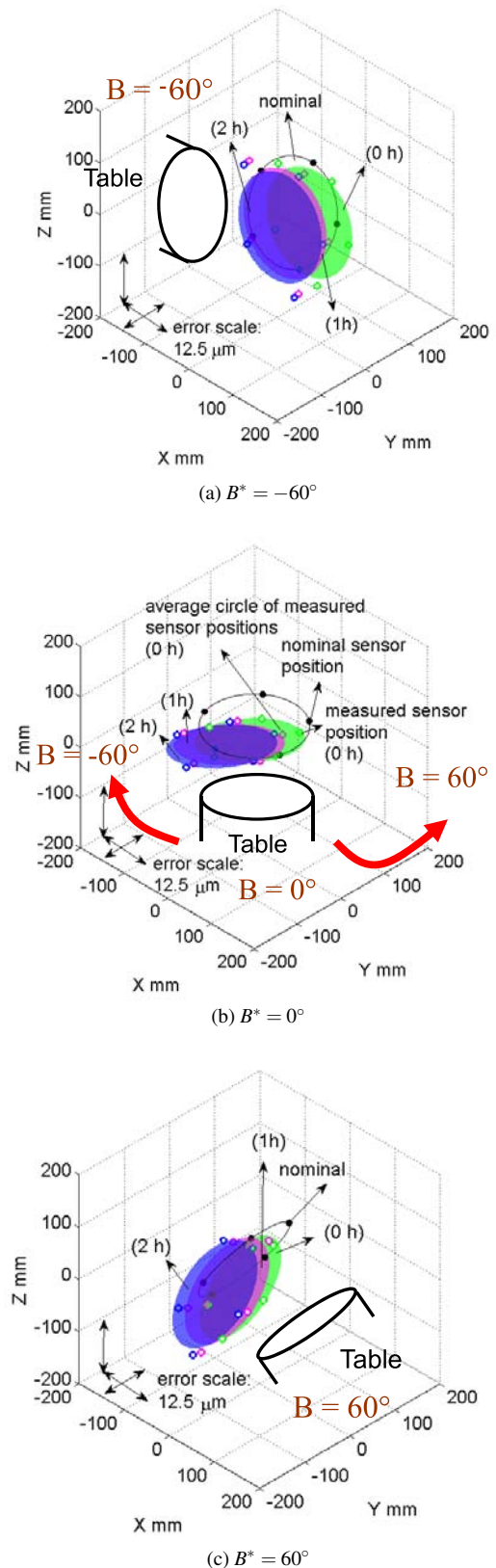
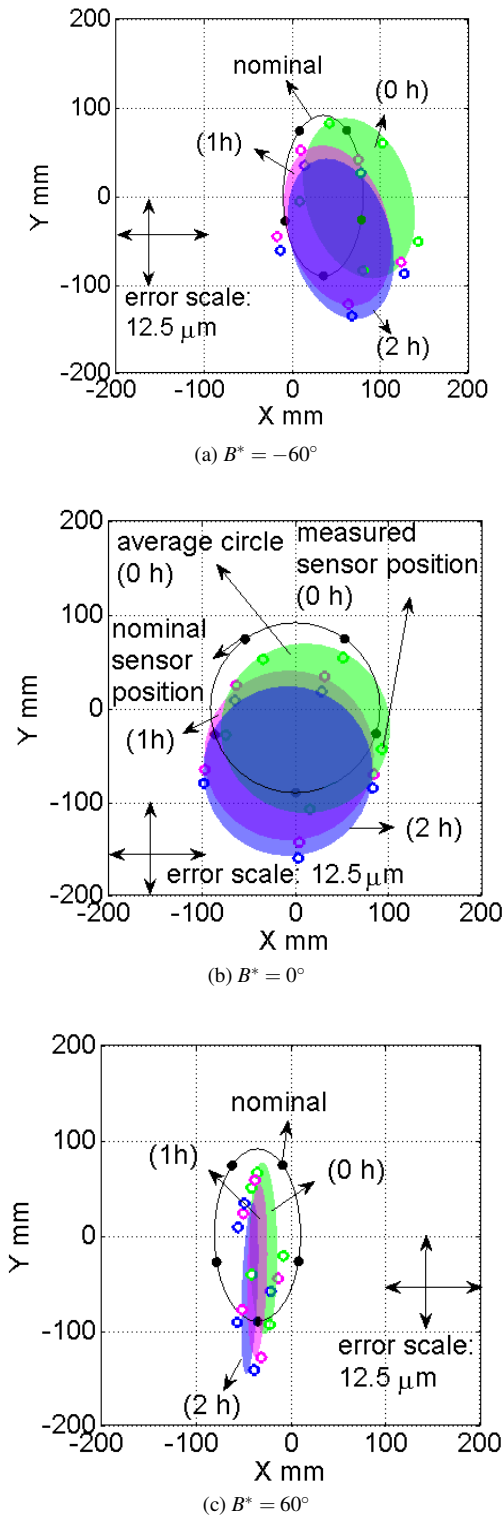
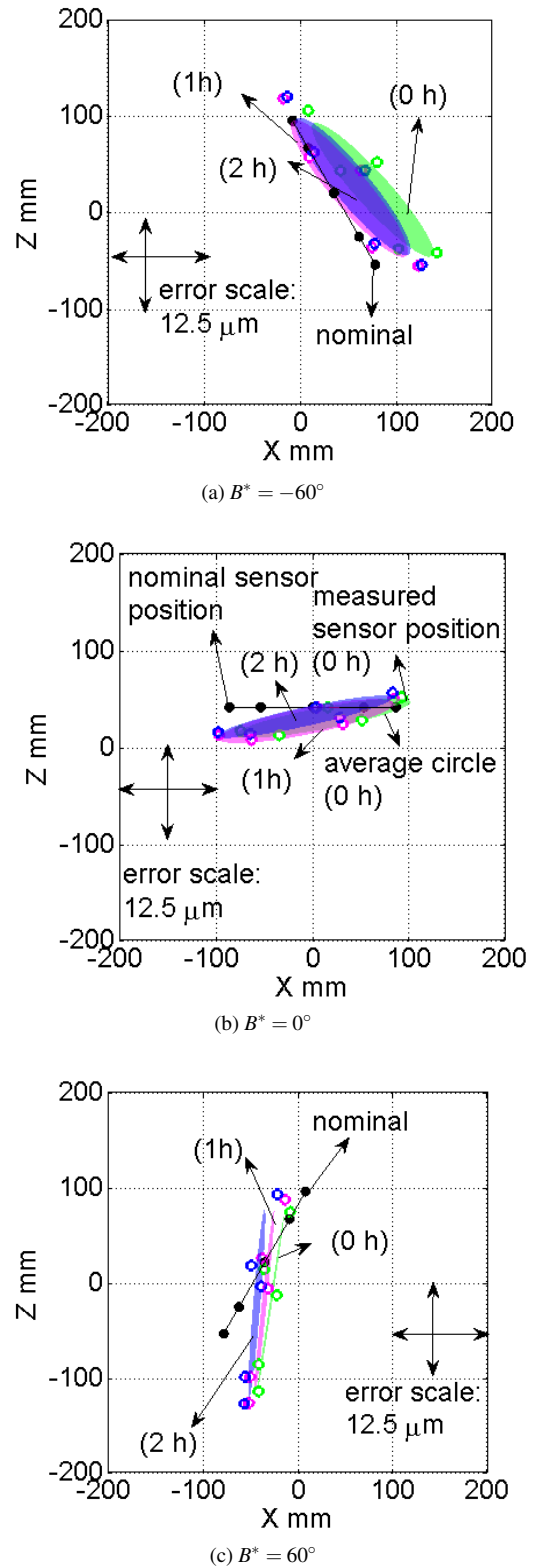


Fig. 7. Sensor positions measured by R-test in the reference coordinate system with *C*-rotation at  $B_i^* = -60^\circ, 0^\circ, 60^\circ$ . An error in a measured sensor position ( $\circ$ ) from its command position ( $\bullet$ ) is magnified 8000 times.



**Fig. 8.** Sensor positions measured by R-test in the reference coordinate system with  $C$ -rotation at  $B_i^* = -60^\circ, 0^\circ, 60^\circ$  projected onto the  $XY$  plane.



**Fig. 9.** Sensor positions measured by R-test in the reference coordinate system with  $C$ -rotation at  $B_i^* = -60^\circ, 0^\circ, 60^\circ$  projected onto the  $XZ$  plane.

ments (i.e.,  $t = 0$  h) is numerically eliminated from the R-test profile in these plots since it is typically caused by miscalibration of the tool length and thus is not regarded as the machine's error motions [16, 17]. The change with time of this axis shift of the  $C$ -table to the  $Z$ -direction is

shown. These plots clearly show the position and orientation of the  $C$ -axis average line at each  $B_i^*$  and how they change as time proceeds.

## (2) Observations

The following observations can be made:

- In **Figs. 8(a)–(c)**, the measured sensor positions move to the  $(-X, -Y)$  direction as time proceeds (about  $-2 \mu\text{m}$  to the  $X$ -direction and  $-6 \mu\text{m}$  to the  $Y$ -direction in 3 hours). This suggests that the temperature rise gradually shifted the position of the axis average line of the  $C$ -axis.
- In **Fig. 9(b)**, a gradual shift of the measured trajectories to the  $Z$ -direction can be observed, although it is significantly smaller than the shift to the  $Y$ -direction. In this machine, the influence of heat in the  $B$ -axis motor mainly affects the rotary table position in the  $Y$ -direction, not in the  $X$ - or  $Z$ -directions.
- In **Fig. 9(b)**, the measured sensor positions are tilted from the nominal trajectory around the  $Y$ -axis. This suggests a squareness error of the  $C$ -axis average line to the  $X$ -axis (see **Fig. 3(b)**), which can be caused by an angular positioning error of the  $B$ -axis at  $B = 0^\circ$ . This orientation error is larger in the measured profiles shown in **Fig. 9(c)**. This represents a larger  $B$ -axis angular positioning error at  $B = 60^\circ$  than at  $B = 0^\circ$ , which can be also observed from **Fig. 8(c)**. A slight change in this angular positioning error with the temperature rise can be observed, although it is not significantly large.

It is important to note that the observations above assume that the error motions of the linear axes are sufficiently small, and thus the errors observed in **Figs. 7–9** are caused by rotary axes error motions only. When this assumption is not met, error profiles are influenced by not only the error motions of the rotary axes but also those of the linear axes. Analogously to many other five-axis calibration schemes presented in the literature (e.g., the ball bar [2] or artifact-based calibration using a touch trigger probe [18]), the R-test only measures the relative displacement of the spindle tip to the table, and it is therefore not possible, in principle, to separate the error motions of the rotary axes and linear axes. In the present thermal test, however, it can be reasonably assumed that the heat transfer to the linear axes is limited (see section 4.2) and thus the thermal influence on their error motions is sufficiently small.

## 4.4. Calibration of Geometric Errors of the Rotary Table

From the R-test results presented in section 4.3, the position and orientation of the  $C$ -axis average line at each  $B_i^*$  can be calculated. Six geometric error parameters of the rotary table, shown in **Table 2**, can be parameterized from the position and orientation of the average circles of the measured sensor positions shown in **Figs. 7–9**. **Figs. 10(a)–(f)** show how the calibrated geometric error parameters change as time proceeds. The identification results tell that:

- The gradual shift of the rotary table in the  $X$ - and  $Y$ -directions observed in the previous subsection is parameterized by a gradual change in  $\delta x_{BY}$  and  $\delta y_{CB}$  in **Figs. 10(a)** and **(b)**.
- From the identified result for  $\delta z_{BY}$  shown in **Fig. 10(c)**, a gradual shift in the  $Z$ -position of the  $B$ -axis centerline is also observed (about  $-2 \mu\text{m}$  in 3 hours) as time proceeds.
- Compared to the measurement uncertainty of the R-test device (estimated to be about  $2 \mu\text{m}$  [9]), the influence of thermal distortion of the machine tool on the tilt error motion of the  $B$ -axis (i.e.,  $\alpha_{BY}$ ,  $\beta_{BY}$ , and  $\gamma_{BY}$ ) in **Figs. 10(d)–(f)** is relatively small, which can also be observed from **Figs. 8** and **9**. However, a slight change in the tilt error motions of the  $B$ -axis was identified, particularly in the tilt error motion around the  $Z$ -axis ( $\gamma_{BY}$ ).

## 5. Conclusion

By introducing an approach proposed in [17] and [16], a calibration method for thermally-induced geometric errors of the  $C$ -axis caused by reciprocating movements of the  $B$ -axis was proposed in this paper.

An example of its experimental application was demonstrated. The present thermal test clarifies how the error motions of the rotary table change with time. From experimental results, the following observations are made:

- The temperature rise of the  $B$ -shaft mainly caused a gradual position shift in the  $C$ -axis average line. Such a shift may potentially cause significant geometric errors in a finished workpiece by five-axis machining [19].
- R-test results clarified the orientation errors in the  $C$ -axis average line that varied with  $B$ -rotation due to reciprocated motion of the  $B$ -axis. A slight change in this tilt error motion was observed, particularly in the tilt error motion around the  $Z$ -axis, which is potentially caused by the thermal influence of the  $B$ -axis.

## Acknowledgements

The machining center used in the present experiments was loaned from the Machine Tool Technologies Research Foundation (MT-TRF) through Equipment on Loan Award Program. This work is in part supported by a grant from Mitsutoyo Association for Science and Technology (MAST). It is also in part supported by the JSPS Grants-in-Aid for Scientific Research (#23560122).

## References:

- [1] S. Ibaraki and W. Knapp, "Indirect Measurement of Volumetric Accuracy for Three-axis and Five-axis Machine Tools: A Review," *Int. J. of Automation Technology*, 6-2, 2012. (in print)

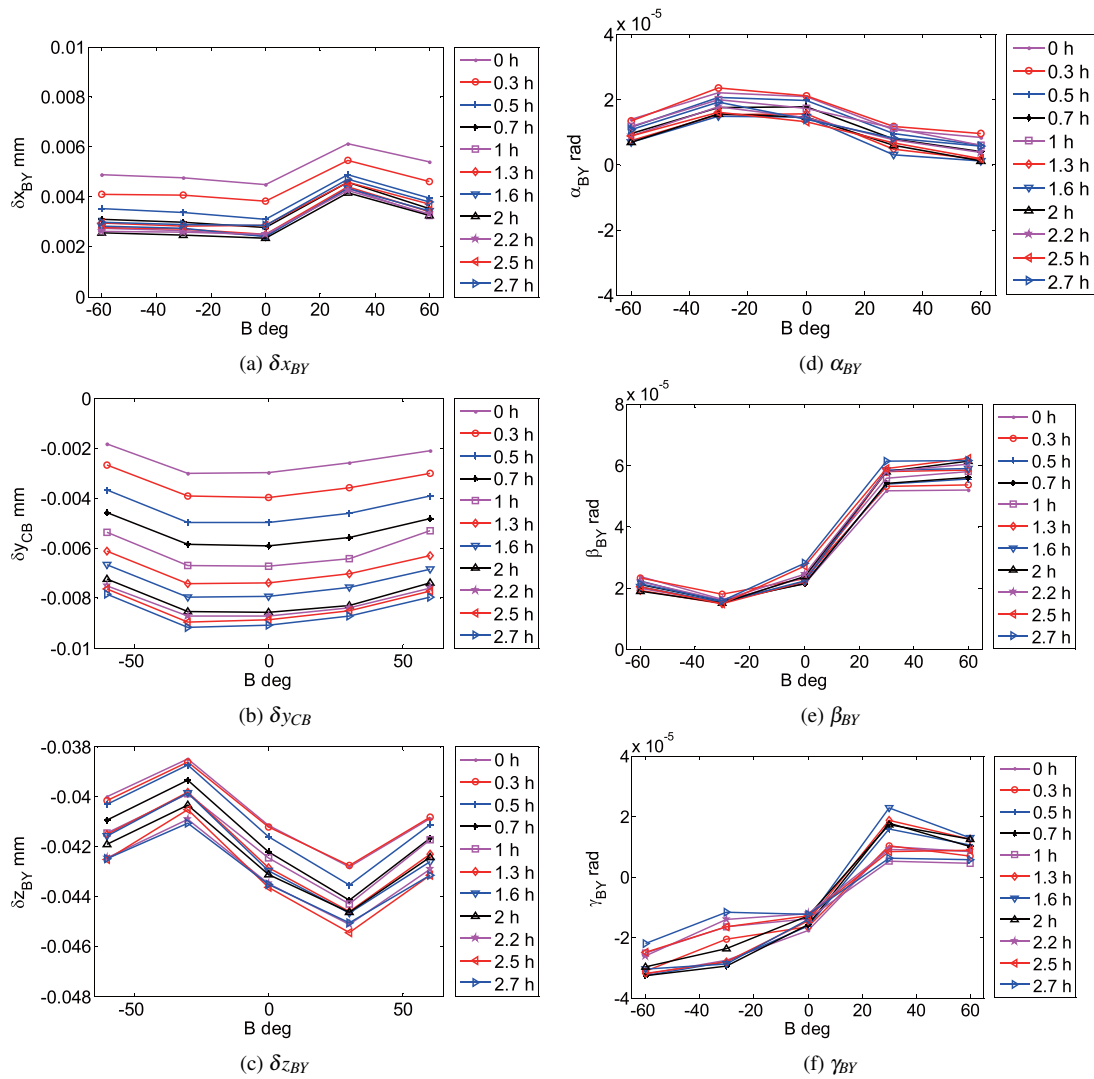


Fig. 10. Calibrated geometric errors of the rotary table at each time interval (See Table 2).

[2] M. Tsutsumi and A. Saito, "Identification and Compensation of Systematic Deviations Particular to 5-axis Machining Centers," *Int. J. of Machine Tools and Manufacture*, 43, pp. 771-780, 2003.

[3] S. H. H. Zargarbashi and J. R. R. Mayer, "Assessment of Machine Tool Trunnion Axis Motion Error, Using Magnetic Double Ball Bar," *Int. J. of Machine Tools and Manufacture*, 46, pp. 1823-1834, 2006.

[4] R. Ramesh, M. A. Mannan, and A. N. Poo, "Error Compensation in Machine Tools – a Review Part II: Thermal Errors," *Int. J. of Machine Tools and Manufacture*, 40, pp. 1257-1284, 2000.

[5] H. Schwenke, W. Knapp et al., "Geometric Error Measurement and Compensation of Machines – An Update," *Annals of the CIRP*, 57-2, pp.560-575, 2008.

[6] ISO 230-3, "Test Code for Machine Tools – Part 3: Determination of Thermal Effects," 2007.

[7] ISO 10791-10, "Test Conditions for Machining Centers – Part 10: Evaluation of Thermal Distortions," 2007.

[8] A. K. Srivastava, S. C. Veldhuis, and M. A. Elbestawit, "Modeling Geometric and Thermal Errors in a Five-axis CNC Machine Tool," *Int. J. of Machine Tools and Manufacture*, 35-9, pp. 1321-1337, 1995.

[9] S. Weikert, "R-Test, a New Device for Accuracy Measurements on Five Axis Machine Tools," *Annals of the CIRP*, 53-1, pp. 429-432, 2004.

[10] B. Bringmann and W. Knapp, "Model-based 'Chase-the-Ball' Calibration of a 5-axis Machining Center," *Annals of the CIRP*, 55-1, pp. 531-534, 2006.

[11] ISO/CD 10791-6:2011, "Test Conditions for Machining Centers – Part 6: Accuracy of Speeds and Interpolations," 2011.

[12] IBS Precision Engineering: <http://www.ibspe.com>.

[13] Fidia: <http://www.fidia.it>.

[14] S. H. H. Zargarbashi and J. R. R. Mayer, "Single Setup Estimation of a Five-axis Machine Tool Eight Link Errors by Programmed End Point Constraint and On-the-fly Measurement with Capball Sensor," *Int. J. of Machine Tools and Manufacture*, 49-10, pp. 759-766, 2009.

[15] ISO 230-7, "Test Code for Machine Tools – Part 7: Geometric Accuracy of Axes of Rotation," 2006.

[16] S. Ibaraki, C. Oyama, and H. Otsubo, "Construction of an Error Map of Rotary Axes on a Five-axis Machining Center by Static R-test," *Int. J. of Machine Tools and Manufacture*, Vol.51, pp. 190-200, 2011.

[17] S. Ibaraki, C. Hong, and C. Oyama, "Construction of an Error Map of Rotary Axes on a Five-axis Machining Center by Static R-test," *Proc. of the 6th Int. Conf. on Leading Edge Manufacturing in 21st Century (LEM21)*, 2011.

[18] T. Erkan, J. R. R. Mayer, and Y. Dupont, "Volumetric Distortion Assessment of a Five-axis Machine by Probing a 3D Reconfigurable Uncalibrated Master Ball Artefact," *Precision Engineering*, 35-1, pp. 116-125, 2011.

[19] C. Hong, S. Ibaraki, and A. Matsubara, "Influence of Position-dependent Geometric Errors of Rotary Axes on a Machining Test of Cone Frustum by Five-axis Machine Tools," *Precision Engineering*, 35-1, pp. 1-11, 2011.



**Name:**  
Cefu Hong

**Affiliation:**  
Department of Micro Engineering, Graduate  
School of Engineering, Kyoto University

**Address:**  
Yoshida-honmachi, Sakyo-ku, Kyoto 606-8501, Japan

**Brief Biographical History:**  
2009- Enrolled in Doctoral Course at Department of Micro Engineering,  
Kyoto University

**Main Works:**  
• "Influence of position-dependent geometric errors of rotary axes on a  
machining test of cone frustum by five-axis machine tools," Precision  
Engineering, Vol.35, No.1, pp. 1-11, 2011.

**Membership in Academic Societies:**  
• The Japan Society of Mechanical Engineers (JSME)  
• The Japan Society for Precision Engineering (JSPE)

---



**Name:**  
Soichi Ibaraki

**Affiliation:**  
Associate Professor, Department of Micro Engi-  
neering, Kyoto University

**Address:**  
Yoshida-honmachi, Sakyo-ku, Kyoto 606-8501, Japan

**Brief Biographical History:**  
2006- Associate Professor, Kyoto University  
2001- Research Associate, Kyoto University

**Main Works:**  
• Atsushi Matsubara, Soichi Ibaraki, "Monitoring and Control of Cutting  
Forces in Machining Processes: A Review," Int. J. of Automation  
Technology, Vol.3, No.4, pp. 445-456, 2009.

**Membership in Academic Societies:**  
• The Japan Society for Precision Engineering (JSPE)  
• The Japan Society of Mechanical Engineers (JSME)  
• The Society of Instrument and Control Engineers (SICE)

---